

Geophysical Research Letters®



RESEARCH LETTER

10.1029/2024GL112739

Key Points:

- Biogeophysical radiative forcings and adjustments of European afforestation were quantified using a climate model and radiative kernels
- Radiative adjustments with high signal-to-noise were highly localized, dominated by low cloud cover change, and heavily confined in space and time
- Annual effective radiative forcings were largely driven by surface albedo change

Supporting Information:

Supporting Information may be found in the online version of this article.

Correspondence to:

R. M. Bright,
ryan.bright@nibio.no

Citation:

Bright, R. M., Caporaso, L., Duveiller, G., Piccardo, M., & Cescatti, A. (2025). Biogeophysical radiative forcings of large-scale afforestation in Europe are highly localized and dominated by surface albedo change. *Geophysical Research Letters*, *52*, e2024GL112739. <https://doi.org/10.1029/2024GL112739>

Received 27 SEP 2024
Accepted 16 NOV 2024






Author Contributions:

Conceptualization: Ryan M. Bright
Data curation: Luca Caporaso, Matteo Piccardo
Formal analysis: Ryan M. Bright
Methodology: Ryan M. Bright
Writing – original draft: Ryan M. Bright
Writing – review & editing: Ryan M. Bright, Luca Caporaso, Gregory Duveiller, Matteo Piccardo, Alessandro Cescatti

© 2024. The Author(s).

This is an open access article under the terms of the [Creative Commons Attribution License](https://creativecommons.org/licenses/by/4.0/), which permits use, distribution and reproduction in any medium, provided the original work is properly cited.

Biogeophysical Radiative Forcings of Large-Scale Afforestation in Europe Are Highly Localized and Dominated by Surface Albedo Change

Ryan M. Bright¹ , Luca Caporaso^{2,3} , Gregory Duveiller⁴ , Matteo Piccardo⁵ , and Alessandro Cescatti² 

¹Norwegian Institute of Bioeconomy Research (NIBIO), Ås, Norway, ²European Commission, Joint Research Centre, Ispra, Italy, ³National Research Council of Italy, Institute of BioEconomy, Rome, Italy, ⁴Max Planck Institute for Biogeochemistry, Jena, Germany, ⁵Collaborator of European Commission, Joint Research Centre, Ispra, Italy

Abstract Large-scale re-/afforestation projects afford sizable atmospheric CO₂ removals yet questions loom surrounding their potentially offsetting biogeophysical radiative forcings. Forest area change alters not only the surface albedo but also heat, moisture, and momentum fluxes, which in turn modify the atmosphere's radiative, thermodynamical, and dynamical properties. These so-called radiative forcing “adjustments” have been little examined in re-/afforestation contexts, and many questions remain surrounding their relevance in relation to the instantaneous forcing from the surface albedo change—and whether they can affect Earth's radiative energy balance in regions remote from where the re-/afforestation occurs. Here, we quantified biogeophysical radiative forcings and adjustments from realistically scaled re-/afforestation in Europe at high spatial resolution and found that adjustments with high signal-to-noise were largely confined to only a few months and to the region of re-/afforestation. Adjustments were dominated by perturbed low-level clouds and rarely exceeded $\pm 25\%$ of the annual albedo change forcing.

Plain Language Summary Increased forest area can boost carbon stores in the terrestrial biosphere and benefit global climate. At the same time, this modifies several biogeophysical properties of the surface that impact Earth's energy balance. The extent to which these so-called “biogeophysical” radiative forcings are important has not been comprehensively evaluated, with much of the research focusing on only a single mechanism—or the change to the surface's reflective properties (i.e., its albedo). Other mechanisms can dampen or reinforce the albedo change forcing and can even lead to remote effects, but these are much less understood. Focusing on Europe, we used a regional climate model combined with other analytical tools to quantify these additional mechanisms and understand their relevance in relation to the local forcing caused by surface albedo changes. We found that these other mechanisms rarely manifested in regions outside the region of re-/afforestation, and further, that they are far less important than the forcing attributable to the surface albedo change.

1. Introduction

Enhancing carbon dioxide removal (CDR) through re-/afforestation (henceforth afforestation) is now widely considered necessary to combat residual emissions and meet ambitious global warming mitigation targets (Griscom et al., 2019; Griscom et al., 2017; Seddon et al., 2020). Current estimates of the mitigation potential of large-scale forestry projects are restricted to carbon cycle impacts (Bastin et al., 2019; Cook-Patton et al., 2020; Griscom et al., 2017; Roebroek et al., 2023; Walker et al., 2022), yet changes to both the vegetation composition and its structure at the land surface alter fluxes of heat, moisture, and momentum—which in turn modify the radiative, thermodynamical, and dynamical properties of the atmosphere resulting in additional so-called “biogeophysical” (BGP) climate forcings (Bonan, 2008; Mahmood et al., 2013; Pielke Sr. et al., 2011). These additional and often non-trivial BGP climate forcings can either enhance or counteract CDR benefits, and excluding them from impact assessments risks the promotion of forestry projects yielding undesirable (at worst) or sub-optimal (at best) climate outcomes.

Empirical investigations of large-scale afforestation have only recently started including BGP forcings by considering the instantaneous shortwave radiative forcing connected to a surface albedo change (Hasler et al., 2024; Rohatyn et al., 2023). However, additional radiative flux perturbations at the top-of-the-atmosphere

(TOA) arising from changes to atmospheric temperatures, humidities, and clouds remain largely excluded or overlooked. These so-called radiative forcing “adjustments” (P Forster et al., 2021; Myhre et al., 2013) are important to consider since they can either dampen or reinforce the instantaneous radiative forcing (*IRF*) that is attributable to the surface albedo change (Andrews et al., 2017; Smith, Kramer, & Sima, 2020). Insights from recent empirical analyses have implicated forests, for instance, as being important controls of low-level convective cloud cover in many regions (Cerasoli et al., 2021; Duveiller et al., 2021; Xu et al., 2022), suggesting that forest area expansion in these regions might lead to cloud adjustments and hence impacts on Earth’s radiative energy balance above and beyond that from a perturbed surface albedo (L’Ecuyer et al., 2019).

Yet large knowledge gaps surrounding the forcing adjustments in the context of large scale afforestation exist—including the relative importance of differing physical mechanisms underlying them, their magnitudes relative to the (albedo change-driven) forcing, and whether they manifest in regions that are remote from the region of afforestation.

Within the climate science community, the classical framework for understanding climate change involves an external forcing, a climate system response that opposes the forcing to regain equilibrium, and feedbacks that dampen or amplify the response (Sherwood et al., 2015). The definition of “external forcing” in this framework has rapidly evolved over the past 10 years in favor of the “effective radiative forcing” (*ERF*) in which the adjustments are defined *as part of the forcing* rather than as a feedback (P Forster et al., 2021; Myhre et al., 2013; Quaas et al., 2024). Compared to other definitions based on the *IRF* or the stratospherically adjusted radiative forcing (*SARF*), the *ERF* is thought to be a better indicator of the climate response over the longer-term (Hansen et al., 2005; Joshi et al., 2003; Richardson et al., 2019). However, *ERFs* from land use/land cover change forcings (like afforestation) have received little scientific attention relative to other forcing agents (e.g., CO₂ and other well-mixed greenhouse gases, sulfate aerosols, black carbon, etc.) (P Forster et al., 2021).

Coupled land-atmosphere (or climate) models are seen as useful tools for addressing these gaps because of their ability to resolve changes to thermodynamical, dynamical, and radiative processes in the atmosphere that accompany the surface biogeophysical property changes. Regional studies in particular are attractive since they permit models to be run in high spatial resolution which is critical for resolving convective-driven cloud formation processes. Here, we employ a convective-permitting version of the RegCM5 regional climate model (Giorgi et al., 2023) together with a suite of radiative kernels (Soden et al., 2008) to diagnose radiative forcings and adjustments (collectively as *ERF*) connected to realistically scaled afforestation in Europe. Specifically, we seek answers to the following questions: Where and when are the adjustments statistically robust? What are the most important adjustment types or mechanisms? What are their magnitudes relative to the *IRF*? What is the relevance of dynamical adjustments leading to remote (non-local) radiative forcing?

2. Methods and Data

2.1. Climate Modeling

Simulations were executed using the non-hydrostatic version of the regional climate model RegCM5 (Giorgi et al., 2023), driven at its lateral boundaries in a one-way nesting setup using a 6-hourly time series of sea surface temperature, surface pressure, wind, temperature, and specific humidity on pressure levels from ERA-5 reanalysis at 0.25° resolution (Hersbach et al., 2020). The grid was defined in Cartesian coordinates at 5 km horizontal resolution, chosen because the model was demonstrated to sufficiently resolve convective cloud processes in Europe at this resolution (Giorgi et al., 2023). Lateral boundary conditions were implemented using an exponential relaxation procedure with a buffer zone width of 40 grid points (Giorgi et al., 1993) without internal nudging. The model used the Zeng Ocean Air-Sea scheme (Zeng et al., 1998) to parametrize air-sea exchanges, while clouds were explicitly simulated using the Single-Moment 5-class microphysics scheme of the WRF model (Skamarock et al., 2008). For the representation of land surface processes, RegCM5 was fully coupled to CLM 4.5 (Oleson et al., 2013) and run with prescribed phenology based on MODIS products (Lawrence & Chase, 2007). Integration time steps were 30 s while outputs were written and saved at a bi-hourly frequency. The model was initialized with ERA-5 meteorological fields on 1 October 2003; the first 3 months (October-December) were treated as a spin-up period and discarded from the *ERF* calculation and subsequent analysis of forcing adjustments (Section 2.3).

2.2. Experimental Set-Up

We executed two simulations: (a) a control run (CTL) with land cover prescribed as the state in 2005 (Lawrence & Chase, 2007), and (b) a second run (FOR) where forest cover on the vegetated land unit was increased at the expense of other vegetation, maintaining the relative percentages of forest plant functional types (PFTs). In the event a grid cell had no forest cover, we extrapolated the relative percentages from the nearest grid cell, removing grass, crop, shrub, and bare soil PFTs prioritized in that order. Forest cover increases (ΔFC) were capped at 30% of the vegetated land unit area unless the forested area already exceeded 70% of the vegetated unit (common in northern Europe) in which case the full extent became a forest. The 30% cap was deemed a good balance between a magnitude needed to generate a sizable signal and that which might be feasible given the general trend in agricultural land abandonment throughout Europe (Ceaușu et al., 2015). Because we preserved the current vegetation cover distribution in CTL and capped ΔFC in FOR, we deemed this set-up to be more realistic than idealized afforestation studies in which the entire vegetation extent is changed from pure non-forest to pure forest (e.g. (Davin et al., 2020)).

Because of our interest in remote forcings—that is, to TOA radiative perturbations over grid cells with no afforestation— ΔFC was limited to every other grid cell and implemented in a checkboard-like pattern (i.e., 0%–30%–0%–30% etc.). However, several of the 0% grid cells ended up acquiring small amounts of forest cover change due to unanticipated spatial re-projections occurring within RegCM5 prior to simulation. We therefore defined grid cells with $\Delta FC < 1\%$ as those where only the remote effects were present.

2.3. Effective Radiative Forcing (ERF) and Forcing Adjustments

Standards to diagnose *ERF* from climate model output (for example, RFMIP (Pincus et al., 2016);) involve differencing monthly averaged TOA radiative fluxes between a perturbation and a control simulation in which sea surface temperatures and ice fractional coverages are prescribed identically in both:

$$ERF = \Delta N = \Delta LW + \Delta SW \quad (1)$$

where ΔN is the net monthly radiative flux difference at TOA (positive downward) or the sum of the long- (ΔLW) and shortwave (ΔSW) radiative flux differences between FOR and CTL.

Simulation (or integration) length is often 30 years, although shorter periods are deemed acceptable if the integration length can constrain forcing uncertainty to $\sim 0.1 \text{ W m}^{-2}$ (P M Forster et al., 2016). Our goal was to carry out simulations at a costly convection-permitting spatial resolution for a large domain, and an 11-year integration length was found to be a reasonable compromise yielding an uncertainty (as defined in Forster et al., 2016) of 0.13 W m^{-2} for our domain.

The difference between *ERF* and *IRF* represents the net forcing adjustment, where *IRF* was defined as the instantaneous shortwave radiative forcing from the surface albedo change ($\Delta\alpha$) following Smith et al. (2020). Radiative kernels (Shell et al., 2008; Soden et al., 2008)—which relate the change to Earth's radiative balance at TOA to some atmospheric state change—were used to quantify *IRF* and the individual forcing adjustments (A_x):

$$A_x = K_x \Delta x \quad (2)$$

where the adjustment attributable to the state change in x —or A_x —was the product of its radiative kernel (K_x) and the state change (Δx). The *IRF* summed with the adjustments yields the *ERF*:

$$ERF = IRF + A_{ta} + A_{ts} + A_{wv} + A_{cld} + \epsilon \quad (3)$$

where A_{ta} , A_{ts} , A_{wv} , and A_{cld} are the adjustments due to changes in atmospheric temperature, surface temperature, water vapor, and clouds, respectively. Kernel unit changes are 1 K for temperature, the change in specific humidity that maintains constant relative humidity for a temperature increase of 1 K for water vapor, and 1% additive for surface albedo. For water vapor, state differences are taken for the logarithm of water vapor concentration following (Sanderson & Shell, 2012; Smith et al., 2018).

Cloud adjustments are estimated using a kernel masking approach because the radiative effect of vertically overlapping cloud fields is too non-linear for the kernel method (Shell et al., 2008; Soden et al., 2008):

$$A_{clد} = (ERF - ERF^{clr}) - (IRF - IRF^{clr}) - \sum_{X \in [ta, ts, ww]} (A_x - A_x^{clr}) \quad (4)$$

where the subscript “*clr*” denotes a forcing or adjustment in clear-sky conditions.

The final term seen in Equation 3—or ϵ —is a residual term assumed to represent nonlinearities within individual processes or nonlinear interactions among different processes (Feldl & Roe, 2013).

Several kernels exist and differ by their spatial and horizontal resolutions, their underlying radiative transfer modeling, and the background climate states applied in their derivation. Chung & Soden (2015) highlighted how differences in the modeling of radiative transfer can lead to discrepancies among kernels, while more recent analysis pointed to a kernel’s state-dependency as a source of discrepancy (H. Huang and Huang, 2023). To minimize the impact of these uncertainties on the results, we employed nine comprehensive (i.e., all adjustments) and two additional $\Delta\alpha$ -only kernel data sets (Table S1 and Text S1 in Supporting Information S1).

Prior to application, the kernels native horizontal and vertical resolutions (pressure levels) were linearly interpolated to match those of the RegCM5 grid.

2.4. Identifying Robust Forcing Signals

When it comes to diagnosing forcings and adjustments from small perturbations like realistically scaled afforestation, a challenge is to distinguish real forcing signals from noise related to internal climate variability (Winckler et al., 2017). To help overcome this, we followed the guidance provided by Lorenz et al. (2016) when assessing the statistical significance of climate change signals obtained from climate modeling experiments. This entailed a two-step procedure using a one-sample paired *t*-test to first test the null hypothesis formulated as a >5% probability that the net adjustment in any given grid cell and month was zero. We then evaluated the field significance of all rejected null hypotheses in our domain by assessing the false discovery rate (FDR) at a q-value of 5% (i.e., 5% of rejected nulls were truly null) (Benjamini & Hochberg, 1995; Storey, 2002). FDR is robust to spatial correlations in the data (Ivanov et al., 2018; Lorenz et al., 2016; Wilks, 2006). When assessing field significance, we divided our domain into “local” and “remote” regions, defined as all grids cells having $\geq 1\%$ and $< 1\%$ ΔFC , respectively.

We diagnosed (net) adjustments prior to significance testing as the differences between monthly ΔN and spatially optimized monthly *IRF* estimates based on one of 11 possible all-sky $\Delta\alpha$ kernels (see Text S1 for details). The optimization procedure was motivated by the desire to minimize bias introduced by any one (or means of multiple) $\Delta\alpha$ kernels when computing *IRF* since we were unable to execute offline (i.e., “double call”) radiative transfer calculations to diagnose *IRF* (Chung & Soden, 2015; P M Forster et al., 2016).

3. Results

3.1. Which Adjustment(s) Dominated?

Disregarding the distinction between local and remote grid cells, on an annual mean basis SW cloud adjustments (Figure 1a) were the largest in magnitude followed by LW cloud adjustments (Figure 1b), although lower tropospheric warming led to a non-negligible negative adjustment (more outgoing LW radiation to space)—particularly over east-central Europe and the Balkans (Figure 1c). Annual surface temperature (Figure 1d) and water vapor adjustments (Figure 1e) played lesser roles, where A_{ww} was mostly positive and dominated by LW (not shown), and where the sign of A_{ts} followed the spatial pattern of the (sign-reversed) surface temperature change (not shown).

The largest net adjustment on the order of 2 W m^{-2} annually occurred over the alpine regions of Norway and central Europe (Figure 1f; $\sum A$), where signs of both LW and SW cloud adjustments agreed (Figures 1a and 1b; both positive). Large positive $\sum A$ on the order 1 W m^{-2} annually was also found in patches of central, southern, and western Europe, whereas the largest negative $\sum A$ on the order of -1 W m^{-2} was found over the British Isles, northern central, and northeastern Europe (Figure 1f). For most of these regions the signs of the two cloud adjustments also tended to align (Figures 1a and 1b).

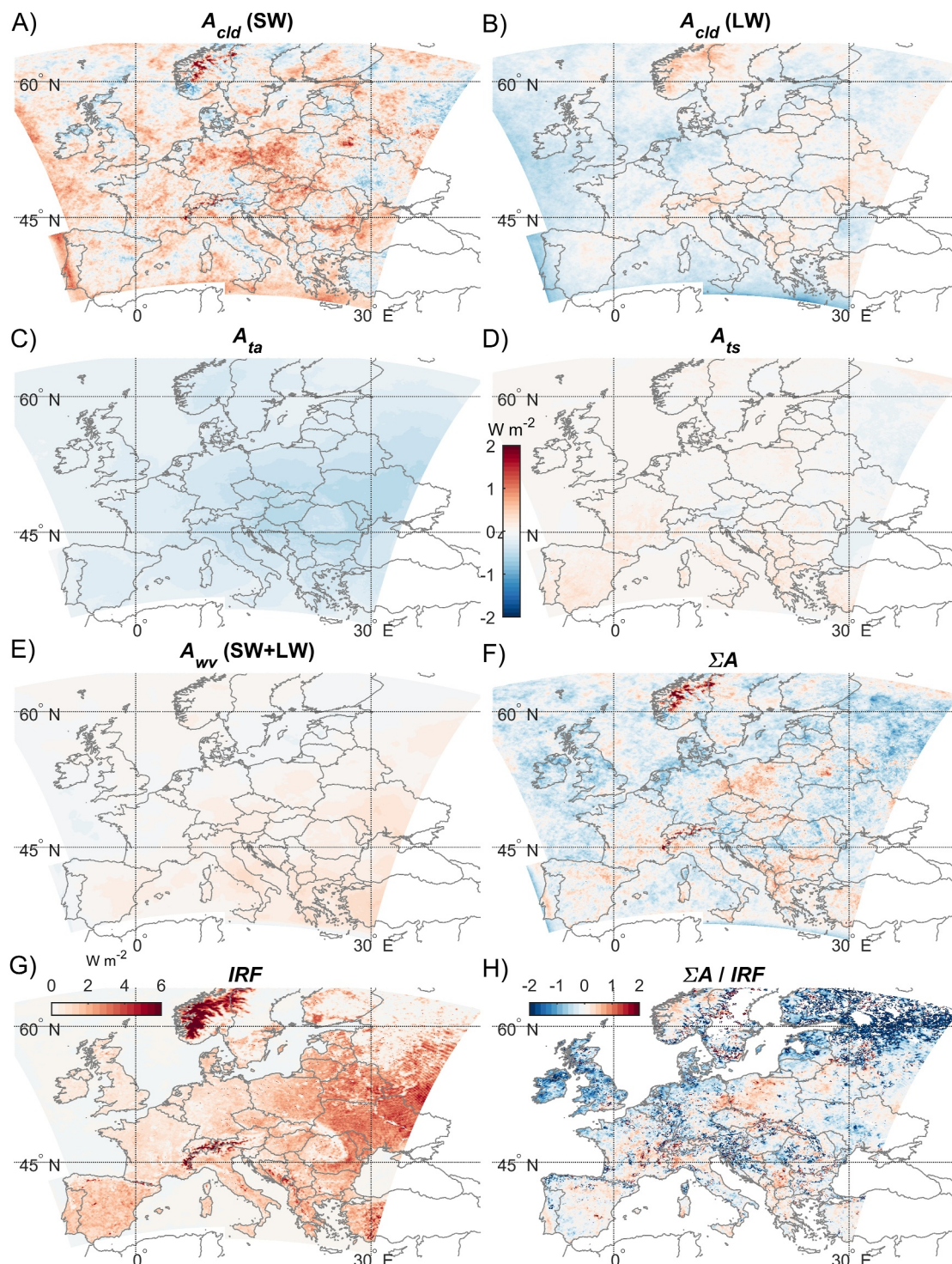


Figure 1. Annual mean: (a) Shortwave (SW) adjustments to cloud property or area changes; (b) Longwave (LW) adjustments to cloud property or area changes; (c) LW adjustments to column air temperature changes; (d) LW adjustments to surface temperature changes; (e) LW and SW adjustments to column water vapor changes; (f) Sum of panels (a)–(e); (g) IRF from $\Delta\alpha$; (h) $\Sigma A/IRF$. Refer to Figure 2A for the underlying forest area perturbations. The colorbar in panel (d) is valid for panels (a)–(f).

The annual IRF (Figure 1g; from $\Delta\alpha$) was mostly positive and largest in regions experiencing high annual solar insolation and long snow cover seasons, such as in eastern Europe and the higher altitude regions. Generally, annual IRF exceeded $1.5 W m^{-2}$ when the perturbed forest area exceeded 10% (Figure 2a). The largest

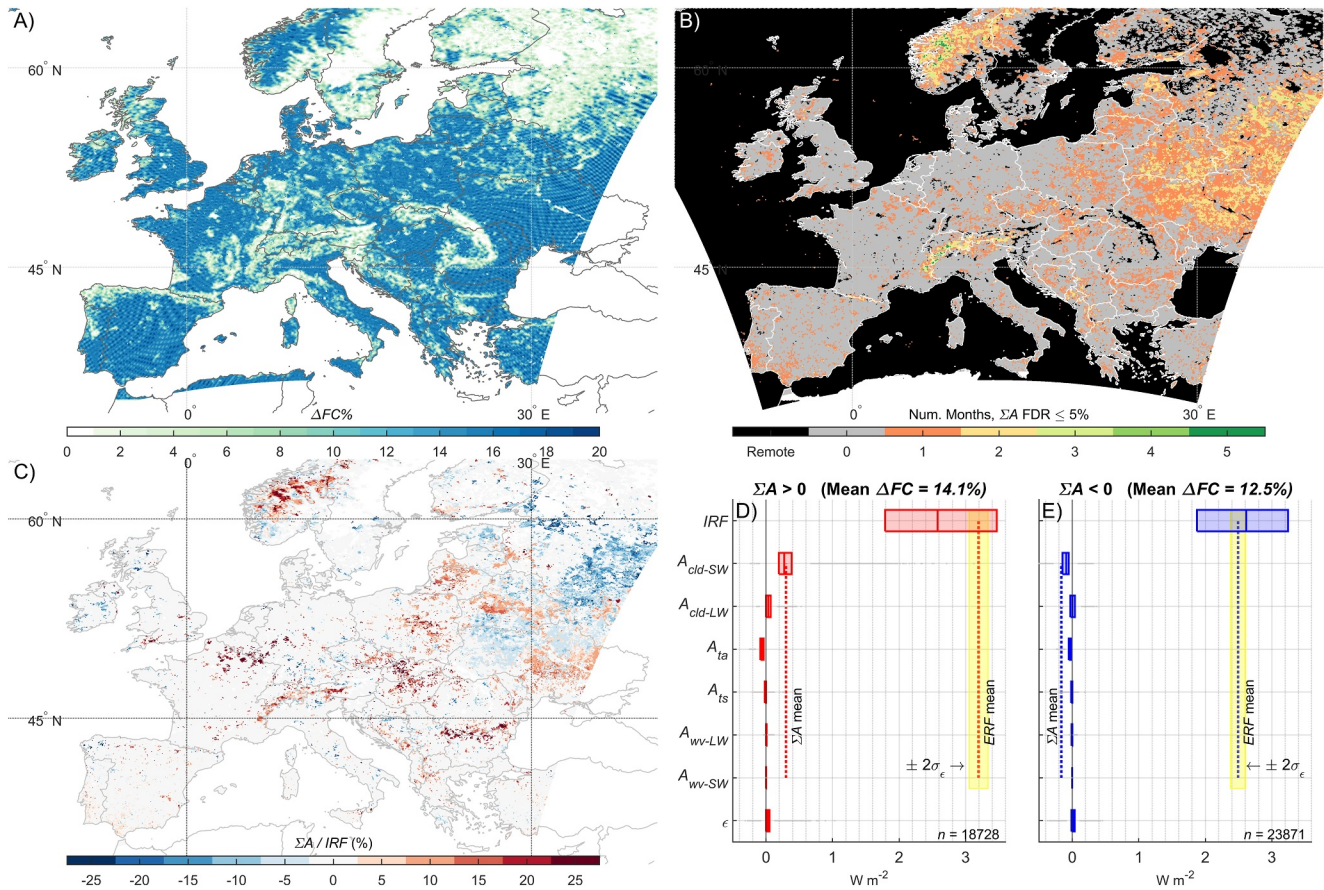


Figure 2. (a) Perturbed forest area as a percentage of grid cell area (land median = 13%; land mean = 10.4%); (b) Spatial distribution of monthly ΣA signals found statistically robust; (c) Annual mean of statistically robust $\Sigma A/IRF$; (d) Annual mean of statistically robust adjustments by mechanism for all afforested grids cells with positive annual ΣA ; (e) Same as in (d) but for afforested grid cells with negative annual ΣA . Boxes in (d) and (e) are interquartile ranges and solid hashes are medians. Yellow bands indicate confidence in the reconstructed ERF —or the sum of the means of all terms in panels (d) and (e) except for the residual term (ϵ).

magnitudes of annual ΣA relative to IRF on the order of -200% were found over the British Isles and north-eastern Europe (Figure 1h).

3.2. Where and When Were Adjustments Statistically Robust?

The spatial extent of adjustments occurring over water bodies in Figure 1 would tend to suggest that afforestation non-negligibly affected atmospheric dynamics. Field significance testing, however, indicated that most of these remote adjustments (i.e., where forest cover perturbations were not imposed or were less than 1%) were simply modeling noise (Figure 2b). Further, field significance testing revealed that most of the adjustments occurring in regions where afforestation *had* been imposed in the model ($\Delta FC \geq 1\%$) were also not statistically robust. Despite relatively homogeneous changes to forest area in most of the land portion of our domain (mean = 10.4%; Figure 2a), statistically robust adjustments (i.e., as $\Sigma A = \Delta N - IRF$) were found in only $\sim 9\%$ of all grid cells in the domain and were relatively heterogeneously distributed and confined largely to just one or two months of the year (Figure 2b, colored grid cells). Statistically robust ΣA occurring remote from the local afforestation was seen in only 152 grid cells (0.03% of domain area). Local surface radiative flux changes and IRF explained $\sim 97\%$ of the temporal-spatial variation in statistically robust ΣA (Text S2 and Table S2 in Supporting Information S1)—including in regions like northeastern Europe with a high concentration of proximal non-perturbed area—reinforcing the finding from the field significance testing that adjustments were highly localized.

Surprisingly, statistically robust ΣA were largely confined to months and locations where transpiration played little role, such as January—March for eastern Europe, January—April for the alpine regions of central Europe, and February—May for alpine Norway (Figure S3 in Supporting Information S1). 85% of all statistically robust

adjustments occurred in January, February, and March. Only for the southern portion of the Iberian peninsula did we find statistically robust $\sum A$ in summer (i.e., July).

3.3. How Did the Statistically Robust Adjustments Scale With IRF ?

Keeping our attention only on the locations where statistically robust adjustment signals were identified in at least 1 month (Figure 2b, orange-to-green pixels), their importance annually could be gauged after normalizing to the annual mean IRF upon setting months with non-statistically robust $\sum A$ equal to zero. No clear spatial pattern in the sign of the annual $\sum A/IRF$ emerged (Figure 2c); positive and negative values occurred at 47% and 53% of statistically robust adjustment locations, respectively. Although small area patches having negative $\sum A/IRF$ could be found sporadically distributed throughout the domain, the largest continuous areas were found in eastern-northeastern Europe, which also contained some of the largest magnitudes approaching -25% ; the largest positive annual $\sum A/IRF$ magnitudes emerged in the Scandic Alps, central, and southeast Europe, where values approaching 25% were found. While positive $\sum A/IRF$ values were found in fewer grid cells, their magnitudes were generally greater than at negative $\sum A/IRF$ locations, made visible by comparing panels D and E in Figure 2 where annual local adjustments were on average 0.30 W m^{-2} (9% of annual IRF) and -0.16 W m^{-2} (-5% of annual IRF), respectively. However, in the months they occurred $\sum A$ could exceed $\pm 100\%$ of the IRF (Text S3 and Fig. S5).

Figures 2d and 2e also reveal that SW cloud adjustments (A_{cld-SW}) dominated the annual mean $\sum A$ while the other adjustments emerged as relatively negligible and partially offsetting of each other, some of which (e.g., A_{wv}) being smaller than the median ϵ —or the proportion of $\sum A$ (as $\Delta N - IRF$) that could not be explained by kernel reconstruction. Median positive A_{cld-SW} was larger than median negative A_{cld-SW} thus explaining why positive $\sum A/IRF$ magnitudes were generally larger.

3.4. What Explained the Sign of the SW Cloud Adjustments?

Changes to cloud area (ΔCLD) at lower altitudes were associated with A_{cld-SW} , where A_{cld-SW} decreased by $\sim 1 \text{ W m}^{-2}$ for every $\sim 1\%$ increase in low-level CLD (Figure 3b)—although changes to cloud optical depths also likely played a role. When binning A_{cld-SW} into 1 W m^{-2} bins, we found that positive A_{cld-SW} bins were associated with large decreases in low-level cloud area close to the surface which could not be compensated by increases to cloud area at higher altitudes (i.e., at lower pressure levels; Figure 3a). While negative A_{cld-SW} bins were also associated with decreased cloud area lower in the planetary boundary layer, these were mostly over-compensated by increases at higher altitudes.

While all bins were found to be associated with cloud gains at higher altitude levels, gained clouds tended to be deeper for the negative A_{cld-SW} bins, with bases starting lower around the 900 hPa level as opposed to around 850 hPa for the positive A_{cld-SW} bins (Figure 3a). Low level ΔCLD patterns mirrored the changes to relative humidities (ΔRH ; Figure 3e), where for the locations experiencing net increases in low-level clouds (i.e., an integral exceeding zero for levels $> 680 \text{ hPa}$) a larger positive ΔRH was generally associated with lower warming (Figure 3c, purple) and greater moistening (Figure 3d, purple) relative to locations experiencing net reductions (Figures 3c–3e, orange).

4. Discussion

4.1. Local Forcings Dominate

When implemented at realistic spatial patterns and intensities within RegCM5-CLM4.5, we found little evidence that European afforestation led to radiative forcings outside the region (i.e., grid cell) of implementation when filtering out modeling noise related to internal climate variability. Robust adjustment signals manifesting remotely from the location of afforestation were identified in only 0.09% of the “remote” area or 0.03% of the total domain area. While this result could have been sensitive to the local significance testing method and the definition of “remote” grid cells, results did not change when basing the local significance testing on Wilcoxon signed rank tests instead of paired t -tests, nor when relaxing the “remote” grid cell definition threshold from $\Delta FC < 1\%$ to $\Delta FC < 5\%$ in an effort to increase the abundance and extent of remote region area. We believe this to be a robust finding, supported by the additional finding that local surface energy balance changes could alone explain $\sim 97\%$ of the spatial-temporal variation in (statistically robust) $\sum A$ throughout the domain (Supporting Text S2 in Supporting Information S1). One would expect this to be lower if perturbations to heat and moisture transport

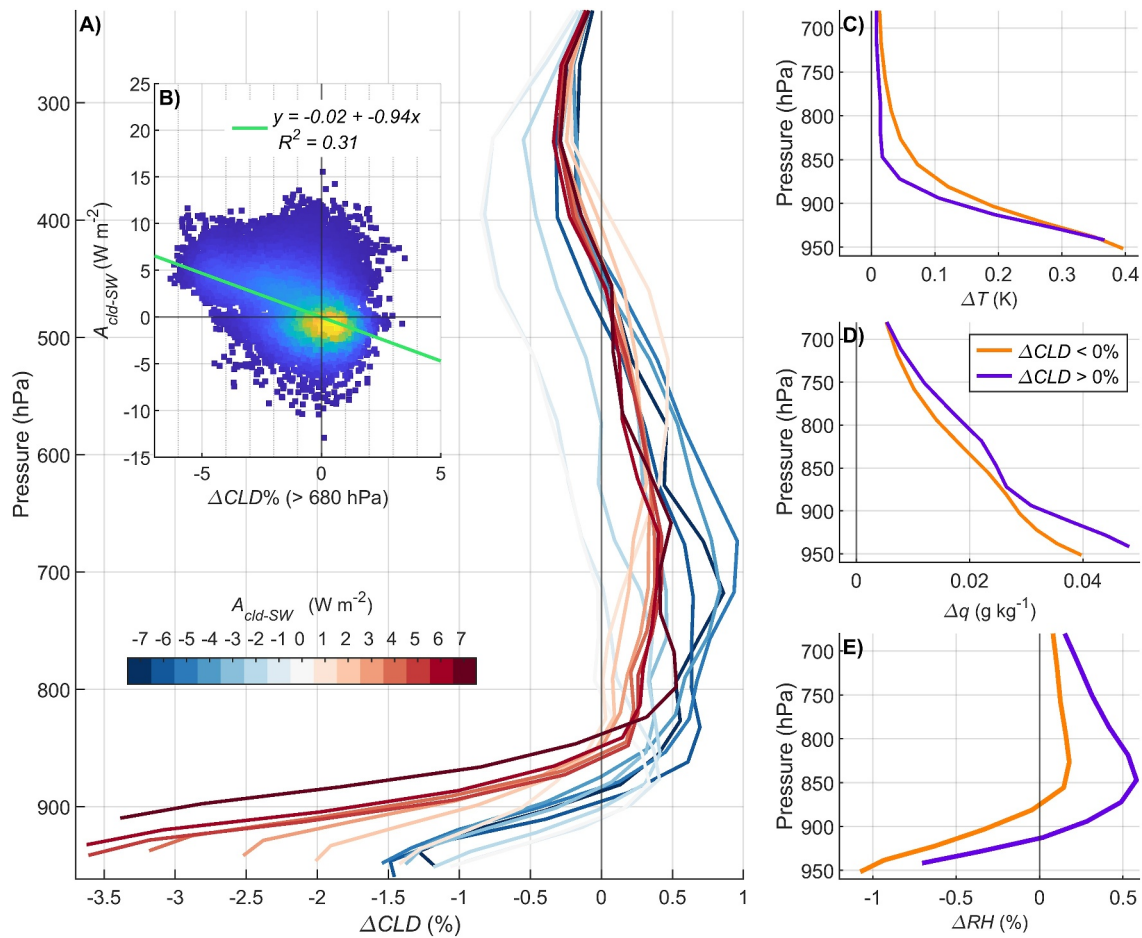


Figure 3. (a) Mean cloud area fraction changes (ΔCLD) following afforestation at altitude levels up to 200 hPa per 1 W m^{-2} A_{cld-sw} bin; (b) A_{cld-sw} as a function of low-level ΔCLD ; Mean changes to temperature (ΔT); (c), specific humidity (Δq); (d), and relative humidity (ΔRH); (e) at altitude levels up to 680 hPa for bins of net positive and net negative ΔCLD at levels >680 hPa.

driving remote signals had played a larger role. The finding that (statistically robust) adjustments—which were dominated by SW cloud adjustments (Figure 2) linked to low-level cloud changes (Figure 3)—occurred mostly over afforested areas aligns with findings reported elsewhere surrounding the high spatial congruity between convective cloud prevalence and the pattern of land cover on the landscape (Duveiller et al., 2021; Lyons, 2002; Rabin et al., 1990; Ray et al., 2003; Xu et al., 2022; Zhong & Doran, 1997). The finding that adjustments were negligible in regions remote from the afforested regions in our domain aligns well with the results reported in Andrews et al. (2017) for the same domain (see Figure 3 therein).

4.2. IRF Dominates ERF

Forcing adjustments were dominated by A_{sw-cld} during winter and spring whose signs and magnitudes were deemed robust when considering the low magnitude of the residual term (ϵ) seen in Figures 2d and 2e. As for the sign of A_{sw-cld} , locations with positive A_{sw-cld} were associated with negative low-level ΔCLD and vice versa (Figure 3a). Surprisingly, A_{sw-cld} were found negligible during the summer growing season and confined to southern Europe during July, which is incongruent with the inferences drawn in recent observational studies about forests' impact on low-level cloud cover during summer months in many European regions (Duveiller et al., 2021; Teuling et al., 2017; Xu et al., 2022). One possible explanation is that the BGP effect is secondary to the role of biogenic volatile organic compounds in determining cloud fractions over forests (Blichner et al., 2024; Petäjä et al., 2022), which was excluded from our modeling but which is inherently included in the observational studies. It is important to point out, however, that results from these and other studies (e.g., Caporaso et al. (2024)) employing space-for-time attribution methods are difficult to compare to our simulated ΔCLD results given the

differences in temporal scoping (i.e., full diel cycle vs. specific points in time) and afforestation magnitudes (i.e., $\Delta FC = \sim 12\% - 16\%$ vs. $\Delta FC = 100\%$).

Although A_{sw-cld} was found to dominate the sign and magnitude of $\sum A$, their confinement to only one or two months of the year (Figure 2b)—and largely to winter/early spring (Figure S3 in Supporting Information S1) when incoming solar radiation was weak—reduced its contribution to the annual *ERF* (Figures 2c–2e). For locations where robust adjustment signals were identified ($\sim 9\%$ of domain area), the mean annual local $\sum A$ was 0.09 W m^{-2} or $\sim 3\%$ of the annual *ERF*, indicating that surface albedo changes (as *IRF*) were far more important in determining the sign and magnitude of *ERF*.

4.3. Limitations and Future Directions

While we employed multiple kernel data sets and a novel *IRF* method to reduce uncertainty surrounding forcing adjustment quantification and their spatio-temporal significance (Text S1 and Figures S2 and S6 in Supporting Information S1), the state changes behind them originated from a single climate model and configuration. While the model we employed (RegCM5) demonstrates good performance in capturing temperature and precipitation patterns across Europe (Coppola et al., 2024), future study with other models is desirable—particularly those that are convection-permitting since these likely confer greater confidence when estimating cloud adjustments. The convection-permitting configuration of RegCM5 we employed, for instance, exhibits improved accuracy in predicting precipitation frequency, intensity, and diurnal cycle relative to a configuration with parameterized convection (Coppola et al., 2024), which is likely owed (in part) to improvements in resolving low-level clouds (Caporaso et al., 2024).

Strong feedbacks between cloud fields (i.e., through cloud cover, cloud base, diabatic processes within the PBL) and the surface energy budget (Betts, 2004; Betts & Viterbo, 2005; Ek & Holtslag, 2004; Santanello et al., 2011; Santanello et al., 2018) complicated our attribution of ΔCLD (and hence A_{sw-cld}) to the perturbed surface fluxes (i.e., the changes to sensible and latent heat fluxes). Attribution efforts using mixing diagrams (Betts, 1992; Betts & Viterbo, 2005; Santanello et al., 2011) or other established metrics of local atmospheric coupling (Santanello et al., 2018) are required to gain better insight into the links between forest cover expansion, perturbed surface energy fluxes, and clouds, and may benefit from working with higher temporal resolution model output data (Findell et al., 2024). Whether sign differences in ΔCLD were related to differences in the turbulent heat fluxes and their underlying biophysical controls at the surface—as opposed to differences in ambient meteorological forcing (Zhong & Doran, 1997)—requires future study.

5. Summary and Conclusions

We carried out convection-permitting regional climate model simulations to quantify the BGP-mediated effective radiative forcing (*ERF*) of spatially extensive yet realistically constrained re-/afforestation in Europe. We then employed radiative kernels to diagnose forcing adjustments and screened for field significance to identify locations and time periods exhibiting robust adjustment signals. From this analysis we conclude the following:

- Robust adjustment signals are highly restricted to the geographic location of afforestation.
- These are dominated by shortwave cloud adjustments, confined to only one or two months during the winter and/or spring.
- Instantaneous radiative forcings (*IRF*) from surface albedo change largely dictate the sign and magnitude of the annual *ERF*.

These findings fill a large gap surrounding the relevance of the BGP-mediated radiative forcing adjustments in relation to *IRF* from surface albedo change linked to afforestation, affirming the importance of sustained research efforts directed toward quantifying albedo change *IRF* while strengthening the merits of recent works comparing *IRF* with carbon sequestration (Bright, Cattaneo, et al., 2024; Hasler et al., 2024).

Conflict of Interest

The authors declare no conflicts of interest relevant to this study.

Data Availability Statement

Atmospheric state change variables (i.e., RegCM5 output) used to assess the statistical robustness of remote adjustments as well as to quantify radiative forcings and adjustments (i.e., as kernel inputs) are available through a Zenodo repository at DOI: 10.5281/zenodo.13847720 (Bright, Caporaso, et al., 2024). See Table S1 in Supporting Information S1 for details surrounding the radiative kernels, including references providing access information.

Acknowledgments

R.M.B. is supported by the Research Council of Norway Grant 302701. G. D acknowledges funding by the European Research Council Grant 855187. L.C. acknowledges funding by the European Commission Grant 31520.

References

- Andrews, T., Betts, R. A., Booth, B. B. B., Jones, C. D., & Jones, G. S. (2017). Effective radiative forcing from historical land use change. *Climate Dynamics*, 48(11), 3489–3505. <https://doi.org/10.1007/s00382-016-3280-7>
- Bastin, J.-F., Finegold, Y., Garcia, C., Mollicone, D., Rezende, M., Routh, D., et al. (2019). The global tree restoration potential. *Science*, 365(6448), 76–79. <https://doi.org/10.1126/science.aax0848>
- Benjamini, Y., & Hochberg, Y. (1995). Controlling the false discovery rate: A practical and powerful approach to multiple testing. *Journal of the Royal Statistical Society - Series B: Statistical Methodology*, 57(1), 289–300. <https://doi.org/10.1111/j.2517-6161.1995.tb02031.x>
- Betts, A. K. (1992). FIFE atmospheric boundary layer budget methods. *Journal of Geophysical Research*, 97(D17), 18523–18531. <https://doi.org/10.1029/91jd03172>
- Betts, A. K. (2004). Understanding hydrometeorology using global models. *Bulletin of the American Meteorological Society*, 85(11), 1673–1688. <https://doi.org/10.1175/bams-85-11-1673>
- Betts, A. K., & Viterbo, P. (2005). Land-surface, boundary layer, and cloud-field coupling over the southwestern Amazon in ERA-40. *Journal of Geophysical Research*, 110(D14). <https://doi.org/10.1029/2004jd005702>
- Blichner, S. M., Yli-Juuti, T., Mielonen, T., Pöhlker, C., Holopainen, E., Heikkinen, L., et al. (2024). Process-evaluation of forest aerosol-cloud-climate feedback shows clear evidence from observations and large uncertainty in models. *Nature Communications*, 15(1), 969. <https://doi.org/10.1038/s41467-024-45001-y>
- Bonan, G. B. (2008). Forests and climate change: Forcings, feedbacks, and the climate benefits of forests. *Science*, 320(5882), 1444–1449. <https://doi.org/10.1126/science.1155121>
- Bright, R. M., Caporaso, L., Duveiller, G., Piccardo, M., & Cescatti, A. (2024). RegCM5 monthly mean differences in atmospheric state variables over Europe, FOR - CTL [Dataset]. *Zenodo*. <https://doi.org/10.5281/zenodo.13847720>
- Bright, R. M., Cattaneo, N., Antón-Fernández, C., Eisner, S., & Astrup, R. (2024). Relevance of surface albedo to forestry policy in high latitude and altitude regions may be overvalued. *Environmental Research Letters*, 19(9), 094023. <https://doi.org/10.1088/1748-9326/ad657e>
- Caporaso, L., Duveiller, G., Giuliani, G., Giorgi, F., Stengel, M., Massaro, E., et al. (2024). Converging findings of climate models and satellite observations on the positive impact of European forests on cloud cover. *Journal of Geophysical Research: Atmospheres*, 129(11), e2023JD039235. <https://doi.org/10.1029/2023jd039235>
- Ceașu, S., Hofmann, M., Navarro, L. M., Carver, S., Verburg, P. H., & Pereira, H. M. (2015). Mapping opportunities and challenges for rewilding in Europe. *Conservation Biology*, 29(4), 1017–1027. <https://doi.org/10.1111/cobi.12533>
- Cerasoli, S., Yin, J., & Porporato, A. (2021). Cloud cooling effects of afforestation and reforestation at midlatitudes. *Proceedings of the National Academy of Sciences*, 118(33), e2026241118. <https://doi.org/10.1073/pnas.2026241118>
- Chung, E.-S., & Soden, B. J. (2015). An assessment of methods for computing radiative forcing in climate models. *Environmental Research Letters*, 10(7), 074004. <https://doi.org/10.1088/1748-9326/10/7/074004>
- Cook-Patton, S. C., Leavitt, S. M., Gibbs, D., Harris, N. L., Lister, K., Anderson-Teixeira, K. J., et al. (2020). Mapping carbon accumulation potential from global natural forest regrowth. *Nature*, 585(7826), 545–550. <https://doi.org/10.1038/s41586-020-2686-x>
- Coppola, E., Giorgi, F., Giuliani, G., Pichelli, E., Ciarlo, J. M., Raffaele, F., et al. (2024). The fifth generation regional climate modeling system, RegCM5: The first CP European-wide simulation and validation over the CORDEX-CORE domains. *ESS Open Archive*, Preprint. <https://essopenarchive.org/doi/full/10.22541/essoar.170542078.180092084>
- Davin, E. L., Rechid, D., Breil, M., Cardoso, R. M., Coppola, E., Hoffmann, P., et al. (2020). Biogeophysical impacts of forestation in Europe: First results from the LUCAS (land use and climate across scales) regional climate model intercomparison. *Earth Syst. Dynam.*, 11(1), 183–200. <https://doi.org/10.5194/esd-11-183-2020>
- Duveiller, G., Filippini, F., Ceglár, A., Bojanowski, J., Alkama, R., & Cescatti, A. (2021). Revealing the widespread potential of forests to increase low level cloud cover. *Nature Communications*, 12(1), 4337. <https://doi.org/10.1038/s41467-021-24551-5>
- Ek, M. B., & Holtslag, A. A. M. (2004). Influence of soil moisture on boundary layer cloud development. *Journal of Hydrometeorology*, 5(1), 86–99. [https://doi.org/10.1175/1525-7541\(2004\)005<0086:iosmob>2.0.co;2](https://doi.org/10.1175/1525-7541(2004)005<0086:iosmob>2.0.co;2)
- Feldl, N., & Roe, G. H. (2013). The nonlinear and nonlocal nature of climate feedbacks. *Journal of Climate*, 26(21), 8289–8304. <https://doi.org/10.1175/jcli-d-12-00631.1>
- Findell, K. L., Yin, Z., Seo, E., Dirmeyer, P. A., Arnold, N. P., Chaney, N., et al. (2024). Accurate assessment of land-atmosphere coupling in climate models requires high-frequency data output. *Geoscientific Model Development*, 17(4), 1869–1883. <https://doi.org/10.5194/gmd-17-1869-2024>
- Forster, P., Storelvmo, T., Armour, K., Collins, W., Dufresne, J.-L., Frame, D., et al. (2021). The earth's energy budget, climate feedbacks, and climate sensitivity. In v. Masson-Delmotte (Ed.), *Climate change 2021: The physical science basis. Contribution of working group I to the sixth assessment report of the intergovernmental panel on climate change* (pp. 923–1054). Cambridge University Press.
- Forster, P. M., Richardson, T., Maycock, A. C., Smith, C. J., Samset, B. H., Myhre, G., et al. (2016). Recommendations for diagnosing effective radiative forcing from climate models for CMIP6. *Journal of Geophysical Research: Atmospheres*, 121(20), 12460–12475. <https://doi.org/10.1002/2016jd025320>
- Giorgi, F., Coppola, E., Giuliani, G., Ciarlo, J. M., Pichelli, E., Nogherotto, R., et al. (2023). The fifth generation regional climate modeling system, RegCM5: Description and illustrative examples at parameterized convection and convection-permitting resolutions. *Journal of Geophysical Research: Atmospheres*, 128(6), e2022JD038199. <https://doi.org/10.1029/2022jd038199>
- Giorgi, F., Marinucci, M. R., Bates, G. T., & De Canio, G. (1993). Development of a second-generation regional climate model (RegCM2). Part II: Convective processes and assimilation of lateral boundary conditions. *Monthly Weather Review*, 121(10), 2814–2832. [https://doi.org/10.1175/1520-0493\(1993\)121<2814:doasgr>2.0.co;2](https://doi.org/10.1175/1520-0493(1993)121<2814:doasgr>2.0.co;2)

- Griscom, B. W., Adams, J., Ellis, P. W., Houghton, R. A., Lomax, G., Miteva, D. A., et al. (2017). Natural climate solutions. *Proceedings of the National Academy of Sciences*, *114*(44), 11645–11650. <https://doi.org/10.1073/pnas.1710465114>
- Griscom, B. W., Lomax, G., Kroeger, T., Fargione, J. E., Adams, J., Almond, L., et al. (2019). We need both natural and energy solutions to stabilize our climate. *Global Change Biology*, *0*(0).
- Hansen, J., Sato, M., Ruedy, R., Nazarenko, L., Lacis, A., Schmidt, G. A., et al. (2005). Efficacy of climate forcings. *Journal of Geophysical Research*, *110*(D18), D18104. <https://doi.org/10.1029/2005jd005776>
- Hasler, N., Williams, C. A., Denney, V. C., Ellis, P. W., Shrestha, S., Terasaki Hart, D. E., et al. (2024). Accounting for albedo change to identify climate-positive tree cover restoration. *Nature Communications*, *15*(1), 2275. <https://doi.org/10.1038/s41467-024-46577-1>
- Hersbach, H., Bell, B., Berrisford, P., Hirahara, S., Horányi, A., Muñoz-Sabater, J., et al. (2020). The ERA5 global reanalysis. *Quarterly Journal of the Royal Meteorological Society*, *146*(730), 1999–2049. <https://doi.org/10.1002/qj.3803>
- Huang, H., & Huang, Y. (2023). Radiative sensitivity quantified by a new set of radiation flux kernels based on the ECMWF Reanalysis v5 (ERA5). *Earth System Science Data*, *15*(7), 3001–3021. <https://doi.org/10.5194/essd-15-3001-2023>
- Ivanov, M., Warrach-Sagi, K., & Wulfmeyer, V. (2018). Field significance of performance measures in the context of regional climate model evaluation. Part 2: Precipitation. *Theoretical and Applied Climatology*, *132*(1), 239–261. <https://doi.org/10.1007/s00704-017-2077-x>
- Joshi, M., Shine, K., Ponater, M., Stuber, N., Sausen, R., & Li, L. (2003). A comparison of climate response to different radiative forcings in three general circulation models: Towards an improved metric of climate change. *Climate Dynamics*, *20*(7–8), 843–854. <https://doi.org/10.1007/s00382-003-0305-9>
- Lawrence, P. J., & Chase, T. N. (2007). Representing a new MODIS consistent land surface in the Community Land Model (CLM 3.0). *Journal of Geophysical Research*, *112*(G1), G01023. <https://doi.org/10.1029/2006jg000168>
- L'Ecuyer, T. S., Hang, Y., Matus, A. V., & Wang, Z. (2019). Reassessing the effect of cloud type on Earth's energy balance in the age of active spaceborne observations. Part I: Top of atmosphere and surface. *Journal of Climate*, *32*(19), 6197–6217. <https://doi.org/10.1175/jcli-d-18-0753.1>
- Lorenz, R., Pitman, A. J., & Sisson, S. A. (2016). Does Amazonian deforestation cause global effects; can we be sure? *Journal of Geophysical Research: Atmospheres*, *121*(10), 5567–5584. <https://doi.org/10.1002/2015jd024357>
- Lyons, T. J. (2002). Clouds prefer native vegetation. *Meteorology and Atmospheric Physics*, *80*(1), 131–140. <https://doi.org/10.1007/s007030200020>
- Mahmood, R., Pielke, R. A., Sr., Hubbard, K. G., Niyogi, D., Dirmeyer, P. A., McAlpine, C., et al. (2013). Land cover changes and their biogeophysical effects on climate. *International Journal of Climatology*, *34*(4), 929–953. <https://doi.org/10.1002/joc.3736>
- Myhre, G., et al. (2013). Chapter 8: Anthropogenic and natural radiative forcing. In K. Tignor, M. Allen, J. Boschung, A. Nauels, Y. Xia, V. Vex, et al. (Eds.), *Climate change 2013: The physical science basis. Contribution of working group I to the fifth assessment report of the intergovernmental panel on climate change* (pp. 659–740). Cambridge University Press.
- Oleson, K., Lawrence, D. M., Bonan, G. B., Drewniak, B., Huang, M., Koven, C. D., et al. (2013). *Technical description of version 4.5 of the community land model (CLM)rep* (p. 434). National Center for Atmospheric Research (NCAR).
- Petäjä, T., Tabakova, K., Manninen, A., Ezhova, E., O'Connor, E., Moisseev, D., et al. (2022). Influence of biogenic emissions from boreal forests on aerosol–cloud interactions. *Nature Geoscience*, *15*(1), 42–47. <https://doi.org/10.1038/s41561-021-00876-0>
- Pielke, R. A., Pitman, A., Niyogi, D., Mahmood, R., McAlpine, C., Hossain, F., et al. (2011). Land use/land cover changes and climate: Modeling analysis and observational evidence. *WIREs Climate Change*, *2*(6), 828–850. <https://doi.org/10.1002/wcc.144>
- Pincus, R., Forster, P. M., & Stevens, B. (2016). The radiative forcing model intercomparison project (RFMIP): Experimental protocol for CMIP6. *Geoscientific Model Development*, *9*(9), 3447–3460. <https://doi.org/10.5194/gmd-9-3447-2016>
- Quaas, J., Andrews, T., Bellouin, N., Block, K., Boucher, O., Ceppi, P., et al. (2024). Adjustments to climate perturbations - Mechanisms, implications, observational constraints. *AGU Advances*, *5*(5), e2023AV001144. <https://doi.org/10.1029/2023AV001144>
- Rabin, R. M., Stadler, S., Wetzel, P. J., Stensrud, D. J., & Gregory, M. (1990). Observed effects of landscape variability on convective clouds. *Bulletin of the American Meteorological Society*, *71*(3), 272–280. [https://doi.org/10.1175/1520-0477\(1990\)071<0272:eoelvo>2.0.co;2](https://doi.org/10.1175/1520-0477(1990)071<0272:eoelvo>2.0.co;2)
- Ray, D. K., Nair, U. S., Welch, R. M., Han, Q., Zeng, J., Su, W., et al. (2003). Effects of land use in southwest Australia: 1. Observations of cumulus cloudiness and energy fluxes. *Journal of Geophysical Research*, *108*(D14). <https://doi.org/10.1029/2002jd002654>
- Richardson, T. B., Forster, P. M., Smith, C. J., Maycock, A. C., Wood, T., Andrews, T., et al. (2019). Efficacy of climate forcings in PDRMIP models. *Journal of Geophysical Research: Atmospheres*, *124*(23), 12824–12844. <https://doi.org/10.1029/2019jd030581>
- Roebroek, C. T. J., Duveiller, G., Seneviratne, S. I., Davin, E. L., & Cescaati, A. (2023). Releasing global forests from human management: How much more carbon could be stored? *Science*, *380*(6646), 749–753. <https://doi.org/10.1126/science.add5878>
- Rohatyn, S., Rotenberg, E., Tatarinov, F., Carmel, Y., & Yakir, D. (2023). Large variations in afforestation-related climate cooling and warming effects across short distances. *Communications Earth & Environment*, *4*(1), 18. <https://doi.org/10.1038/s43247-023-00678-9>
- Sanderson, B. M., & Shell, K. M. (2012). Model-specific radiative kernels for calculating cloud and noncloud climate feedbacks. *Journal of Climate*, *25*(21), 7607–7624. <https://doi.org/10.1175/jcli-d-11-00726.1>
- Santanello, J. A., Dirmeyer, P. A., Ferguson, C. R., Findell, K. L., Tawfik, A. B., Berg, A., et al. (2018). Land–atmosphere interactions: The LoCo perspective. *Bulletin of the American Meteorological Society*, *99*(6), 1253–1272. <https://doi.org/10.1175/bams-d-17-0001.1>
- Santanello, J. A., Peters-Lidard, C. D., & Kumar, S. V. (2011). Diagnosing the sensitivity of local land–atmosphere coupling via the soil moisture–boundary layer interaction. *Journal of Hydrometeorology*, *12*(5), 766–786. <https://doi.org/10.1175/jhm-d-10-05014.1>
- Seddou, N., Chausson, A., Berry, P., Girardin, C. A. J., Smith, A., & Turner, B. (2020). Understanding the value and limits of nature-based solutions to climate change and other global challenges. *Philosophical Transactions of the Royal Society of London B Biological Sciences*, *375*(1794), 20190120. <https://doi.org/10.1098/rstb.2019.0120>
- Shell, K. M., Kiehl, J. T., & Shields, C. A. (2008). Using the radiative kernel Technique to calculate climate feedbacks in NCAR's community atmospheric model. *Journal of Climate*, *21*(10), 2269–2282. <https://doi.org/10.1175/2007jcli2044.1>
- Sherwood, S. C., Bony, S., Boucher, O., Bretherton, C., Forster, P. M., Gregory, J. M., & Stevens, B. (2015). Adjustments in the forcing–feedback framework for understanding climate change. *Bulletin of the American Meteorological Society*, *96*(2), 217–228. <https://doi.org/10.1175/bams-d-13-00167.1>
- Skamarock, W. C., Klemp, J. B., Dudhia, J., Gill, D. O., Barker, D., Duda, M. G., et al. (2008). *A description of the advanced research WRF version 3 (No. NCAR/TN-475+STR)Rep* (p. 125). University Corporation for Atmospheric Research. <https://doi.org/10.5065/D68S4MVH>
- Smith, C. J., Kramer, R. J., Myhre, G., Alterskjær, K., Collins, W., Sima, A., et al. (2020). Effective radiative forcing and adjustments in CMIP6 models. *Atmospheric Chemistry and Physics*, *20*(16), 9591–9618. <https://doi.org/10.5194/acp-20-9591-2020>
- Smith, C. J., Kramer, R. J., Myhre, G., Forster, P. M., Soden, B. J., Andrews, T., et al. (2018). Understanding Rapid adjustments to Diverse forcing agents. *Geophysical Research Letters*, *45*(21), 12023–012031. <https://doi.org/10.1029/2018gl079826>

- Soden, B. J., Held, I. M., Colman, R., Shell, K. M., Kiehl, J. T., & Shields, C. A. (2008). Quantifying climate feedbacks using radiative kernels. *Journal of Climate*, *21*(14), 3504–3520. <https://doi.org/10.1175/2007jcli2110.1>
- Storey, J. D. (2002). A direct approach to false discovery rates. *Journal of the Royal Statistical Society: Series B*, *64*(3), 479–498. <https://doi.org/10.1111/1467-9868.00346>
- Teuling, A. J., Taylor, C. M., Meirink, J. F., Melsen, L. A., Miralles, D. G., van Heerwaarden, C. C., et al. (2017). Observational evidence for cloud cover enhancement over western European forests. *Nature Communications*, *8*(1), 14065. <https://doi.org/10.1038/ncomms14065>
- Walker, W. S., Gorelik, S. R., Cook-Patton, S. C., Baccini, A., Farina, M. K., Solvik, K. K., et al. (2022). The global potential for increased storage of carbon on land. *Proceedings of the National Academy of Sciences*, *119*(23), e2111312119. <https://doi.org/10.1073/pnas.2111312119>
- Wilks, D. S. (2006). On “field significance” and the false discovery rate. *Journal of Applied Meteorology and Climatology*, *45*(9), 1181–1189. <https://doi.org/10.1175/jam2404.1>
- Winckler, J., Reick, C. H., & Pongratz, J. (2017). Robust identification of local biogeophysical effects of land-cover change in a global climate model. *Journal of Climate*, *30*(3), 1159–1176. <https://doi.org/10.1175/jcli-d-16-0067.1>
- Xu, R., Li, Y., Teuling, A. J., Zhao, L., Spracklen, D. V., Garcia-Carreras, L., et al. (2022). Contrasting impacts of forests on cloud cover based on satellite observations. *Nature Communications*, *13*(1), 670. <https://doi.org/10.1038/s41467-022-28161-7>
- Zeng, X., Zhao, M., & Dickinson, R. E. (1998). Intercomparison of bulk aerodynamic algorithms for the computation of sea surface fluxes using TOGA COARE and TAO data. *Journal of Climate*, *11*(10), 2628–2644. [https://doi.org/10.1175/1520-0442\(1998\)011<2628:iobaaf>2.0.co;2](https://doi.org/10.1175/1520-0442(1998)011<2628:iobaaf>2.0.co;2)
- Zhong, S., & Doran, J. C. (1997). A study of the effects of spatially varying fluxes on cloud formation and boundary layer properties using data from the southern great plains cloud and radiation testbed. *Journal of Climate*, *10*(2), 327–341. [https://doi.org/10.1175/1520-0442\(1997\)010<0327:asoteo>2.0.co;2](https://doi.org/10.1175/1520-0442(1997)010<0327:asoteo>2.0.co;2)

References From the Supporting Information

- Block, K., & Mauritsen, T. (2014). Forcing and feedback in the MPI-ESM-LR coupled model under abruptly quadrupled CO₂. *Journal of Advances in Modeling Earth Systems*, *5*(4), 676–691. <https://doi.org/10.1002/jame.20041>
- Bright, R. M., & O'Halloran, T. L. (2019). Developing a monthly radiative kernel for surface albedo change from satellite climatologies of earth's shortwave radiation budget: CACK v1.0. *Geoscientific Model Development*, *12*(9), 3975–3990. <https://doi.org/10.5194/gmd-12-3975-2019>
- Huang, Y., Xia, Y., & Tan, X. (2017). On the pattern of CO₂ radiative forcing and poleward energy transport. *Journal of Geophysical Research: Atmospheres*, *122*(20), 10578–10593. <https://doi.org/10.1002/2017jd027221>
- Kramer, R. J., Matus, A. V., Soden, B. J., & L'Ecuyer, T. S. (2019). Observation-based radiative kernels from CloudSat/CALIPSO. *Journal of Geophysical Research: Atmospheres*, *0*(0). <https://doi.org/10.1029/2018JD029021>
- Myhre, G., Kramer, R. J., Smith, C. J., Hodnebrog, Ø., Forster, P., Soden, B. J., et al. (2018). Quantifying the importance of Rapid adjustments for global precipitation changes. *Geophysical Research Letters*, *45*(20), 11399–11405. <https://doi.org/10.1029/2018gl079474>
- Pendergrass, A. G., Conley, A., & Vitt, F. M. (2018). Surface and top-of-atmosphere radiative feedback kernels for CESM-CAM5. *Earth System Science Data*, *10*(1), 317–324. <https://doi.org/10.5194/essd-10-317-2018>
- Smith, C. J., Kramer, R. J., & Sima, A. (2020). The HadGEM3-GA7.1 radiative kernel: The importance of a well-resolved stratosphere. *Earth System Science Data*, *12*(3), 2157–2168.